DR. TIN LOK WONG (Orcid ID : 0000-0003-1147-7958)

DR. TERENCE K LEE (Orcid ID : 0000-0003-0682-322X)

DR. STEPHANIE KWAI YEE MA (Orcid ID : 0000-0002-2029-7943)

Article type : Original

CRAF methylation by PRMT6 regulates aerobic glycolysis driven hepatocarcinogenesis via ERK-dependent PKM2 nuclear relocalization and activation

Tin-Lok Wong[1], Kai-Yu Ng[1], Kel Vin Tan[3], Lok-Hei Chan[1], Lei Zhou[1], Noelia Che[1], Ruby LC Hoo[5], Terence K Lee[6,7], Stephane Richard[8], Chung-Mau Lo[4], Kwan Man[4], Pek-Lan Khong[3], Stephanie Ma[1,2]

1 School of Biomedical Sciences, Li Ka Shing Faculty of Medicine, the University of Hong Kong, Hong Kong; 2 State Key Laboratory of Liver Research, Li Ka Shing Faculty of Medicine, the University of Hong Kong, Hong Kong; 3 Department of Diagnostic Radiology, Queen Mary Hospital, the University of Hong Kong, Hong Kong; 4 Department of Surgery, Queen Mary Hospital, the University of Hong Kong, Hong Kong; 5 Department of Pharmacology and Pharmacy, Li Ka Shing Faculty of Medicine, the University of Hong Kong, Hong Kong; 6 Department of Applied Biology and Chemical Technology, the Hong Kong Polytechnic University, Hong Kong; 7 State Key Laboratory of Chemical Biology and Drug Discovery, the Hong Kong Polytechnic University, Hong Kong; 8 Segal Cancer Center, Lady Davis Institute, Jewish General Hospital, and Departments of Oncology and Medicine, McGill University, Montréal, Canada.

Correspondence: Dr. Stephanie Ma, PhD, School of Biomedical Sciences, Li Ka Shing Faculty of Medicine, The University of Hong Kong, Room 47, 1/F, Laboratory Block, 21 Sassoon Road, Pokfulam, Hong Kong. E-mail: stefma@hku.hk.

Short title: PRMT6 promotes Warburg effect in HCC via PKM2

Keywords: arginine methylation; hepatocellular carcinoma; Warburg effect; PKM2; PRMT6; cancer metabolism; liver cancer; glycolysis

Conflict of interest: The authors have nothing to disclose.

ABSTRACT

Most tumor cells use aerobic glycolysis (the Warburg effect) to support anabolic growth and promote tumorigenicity and drug resistance. Intriguingly, the molecular mechanisms underlying this phenomenon are not well understood. In this work, using gain- and loss-of-function *in vitro* studies in patient-derived organoid and cell cultures as well as *in vivo* PET-MRI animal models, we showed that PRMT6 regulates aerobic glycolysis in human hepatocellular carcinoma (HCC) through nuclear relocalization of pyruvate kinase M2 isoform (PKM2), a key regulator of the Warburg effect. We found PRMT6 to methylate CRAF at arginine 100, interfere with its RAS/RAF binding potential and as a result alter ERK-mediated PKM2 translocation into the nucleus. This altered PRMT6–ERK–PKM2 signaling axis was further confirmed in both a HCC mouse model with endogenous knockout of PRMT6 as well as in HCC clinical samples. We also identified PRMT6 as a novel target of hypoxia via the transcriptional repressor REST, linking PRMT6 with hypoxia in driving glycolytic events. Finally, we showed as a proof-of-concept the therapeutic potential of using 2-deoxyglucose (2DG), a glycolysis inhibitor, to reverse tumorigenicity and sorafenib resistance mediated by PRMT6 deficiency in HCC. ***Conclusion:*** Our findings indicate that the PRMT6-ERK-PKM2 regulatory axis is an important determinant of the Warburg effect in tumor cells and provide a mechanistic link between tumorigenicity, sorafenib resistance and glucose metabolism.

INTRODUCTION

In the presence of sufficient levels of oxygen, normal cells metabolize glucose via glycolysis to pyruvate, which is further metabolized through mitochondrial oxidative phosphorylation for ATP production; whereas under hypoxic/anaerobic conditions, cells ferment glucose to lactate. In contrast, rapidly dividing cells convert much of the glucose into lactate irrespective of oxygen availability. This cell metabolism, known as aerobic glycolysis or the Warburg effect, allows dividing cells to use intermediary glucose metabolites to generate reducing equivalents and macromolecules required for the doubling of biomass, and to suppress apoptosis (1-2). As such, increased aerobic glycolysis is a widely observed feature in human cancers and often correlates with tumor aggressiveness and poor patient prognosis in many tumor types, including human hepatocellular carcinoma (HCC), which represents the main type of liver cancer (3). Importantly, interference with altered metabolism in tumor cells results in reduced tumorigenicity and increased apoptotic sensitivity to chemotherapeutics suggesting that the aerobic glycolytic metabolism is central to tumor growth and survival. Thus, a better understanding of the mechanistic links between cell metabolism and survival control is of paramount significance for the development of new therapeutics particularly in a disease like HCC, given that the liver is known to be a metabolic hub that is responsible for a number of unique metabolic functions including blood glucose homeostasis.

Pyruvate kinase (PK) is a rate limiting enzyme responsible for catalyzing the final step in glycolysis. There are four PK isoforms encoded by 2 paralogous genes - PKLR and PKM. The PKLR gene generates PKL and PKR isoforms that are driven by different tissue-specific promoters, while the PKM gene is produced by mutually exclusive alternative splicing to generate PKM1 and PKM2. PKM2 is upregulated in multiple cancer types, including HCC, and is well recognized to contribute to the Warburg effect (4-5). Switching PKM2 to PKM1 reverses aerobic glycolysis to oxidative phosphorylation and reduces tumor formation in nude mice (6), identifying PKM2 as a potential cancer therapy target and underscoring the importance of identifying endogenous regulators of PKM2 activation in cancer.

Protein arginine methylation, catalyzed by protein arginine methyltransferase (PRMTs), is a prevalent post-translational modification (7-8). The human genome encodes at least nine different PRMTs. PRMTs catalyze mono- or di-methylation reactions on arginine residues. Because of different catalytic specificities, asymmetric dimethyl-arginine is produced by type 1 PRMTs (PRMT1, PRMT2, PRMT3, PRMT4, PRMT6 and PRMT8) whereas symmetric dimethyl-arginine forms with the help of type II PRMTs (PRMT5 and PRMT9). Protein arginine methylation regulates multiple cellular processes including cellular metabolism, transcription, mRNA translation, and signal transduction (8). The current human and mouse protein methylomes indicate that almost 3% of all metabolic enzymes are modified by arginine methylation (9-10). Notably, clinical evidence suggests that PRMTs are deregulated in various cancers (11-12). These observations do indeed imply that PRMTs potentially modulate nutrient sensing and cancer metabolism by regulating the methylation of metabolic enzymes. And indeed in recent years, there has been a number of studies that have identified a link between protein arginine methylation and aerobic glycolysis in the context of cancer. Yet, studies have been limited to PRMT1 and PRMT4, (13-15); and this area of work remains relatively unexplored.

PRMT6 is a type I PRMT that asymmetrically dimethylates protein substrates including histones, transcriptional factors and co-regulators (8). Previous work from our group have found PRMT6 to be frequently down-regulated and negatively correlated with aggressive cancer features in human HCC. We also demonstrated a critical repressive function for PRMT6 in maintenance of HCC cancer stemness by regulating RAS binding and MEK/ERK signaling via methylation of CRAF on arginine 100 (16). However, whether PRMT6 regulates energy metabolism in cancer cells remains unknown. In this study, using HCC patient-derived organoids and cells *in vitro* and positron emission tomography-magnetic resonance imaging (PET-MRI) analysis of xenografted tumors *in vivo*, we discovered PRMT6 to promote HCC tumor growth and sorafenib resistance by reprogramming oxidative phosphorylation to aerobic glycolysis. Methylation of CRAF at arginine 100 by PRMT6 will alter downstream MEK/ERK signaling, thereby regulating expression and translocation of PKM2 into the nucleus in an ERK-dependent manner. This altered PRMT6–ERK–PKM2 signaling axis was further confirmed in both a HCC mouse model with endogenous knockout of PRMT6 as well as in HCC clinical samples. We also identified PRMT6 as a novel target of hypoxia via the

transcriptional repressor REST, linking PRMT6 with hypoxia in driving Warburg effect. Finally, we showed as a proof-of-concept the therapeutic potential of using 2-deoxyglucose, a glycolysis inhibitor, to reverse tumorigenicity and sorafenib resistance mediated by PRMT6 deficiency in HCC. This study reveals a novel molecular link between a regulator of cell survival and a key enzyme in cancer metabolism with potential therapeutic implications.

MATERIALS AND METHODS

Cell lines and HCC patient-derived organoid cultures. HCC cell line HepG2 were purchased from American Type Culture Collect (ATCC). HCC cell line MHCC97L cells were obtained from Liver Cancer Institute, Fudan University, China. Huh1 was purchased from the Japanese Collection of Research Bioresources Cell Bank (JCRB Cell Bank). 293T and 293T/17 cells were purchased from ATCC; while 293FT was purchased from Invitrogen. Cell lines used in this study were regularly authenticated by morphological observation and tested for absence of Mycoplasma contamination. Authenticity of MHCC97L was validated by STR profiling. For patient-derived organoid cultures, cells were isolated and cultured as previously described (16, 33). HCC tissues used for organoid establishment were obtained from HCC patients undergoing hepatectomy or liver transplantation at Queen Mary Hospital, Hong Kong, with informed consent obtained from all patients and protocol approved by the Institutional Review Board of the University of Hong Kong / Hospital Authority Hong Kong West Cluster. Samples were collected from patients who had not received any previous local or systemic treatment prior to operation.

Clinical samples. Formalin-fixed paraffin-embedded primary human HCC and adjacent non-tumor liver tissue samples were obtained from HCC patients undergoing hepatectomy or liver transplantation at Queen Mary Hospital, Hong Kong, with informed consent obtained from all patients and protocol approved by the Institutional Review Board of the University of Hong Kong / Hospital Authority Hong Kong West Cluster. Samples were collected from patients who had not received any previous local or systemic treatment prior to operation.

Animal tumorigenicity studies. The study protocol was approved by and performed in accordance with the Committee of the Use of Live Animals in Teaching and Research at The University of Hong Kong. Tumorigenicity was determined by subcutaneous injection into the flank of 4-to-5 week old male BALB/C nude mice. Tumor incidence and tumor size/growth were recorded. After tumors were detected, tumor sizes were measured every 2-3 days by calipers and tumor volumes were calculated as volume (cm^3) = L x W^2 x 0.5 with L and W representing the largest and smallest diameters, respectively. Tumors formed were harvested for histological analysis. $PRMT6^{-/-}$ mice were provided by Stéphane Richard (17). $PRMT6^{-/-}$ mice were viable, fertile and did not display any overt phenotype. WT C57BL/6J and $PRMT6^{-/-}$ mice were treated with N-nitrosodiethylamine (DEN, intraperitoneal, 1mg/kg) at the age of 14 days. Starting at 8 weeks of age, carbon tetrachloride (CCl_4, intraperitoneal, 0.2ml/kg) was administered twice weekly for an additional 14 weeks. Livers were harvested for histological analysis.

Animal PET–MRI studies. HCC cells overexpressing EV or PRMT6 were injected orthotopically into the liver of 6-to-7 weeks old male BALB/C nude mice. Four weeks post injection, mice were analyzed on the pre-clinical *nanoScan* PET/MRI system (Mediso Medical Imaging Systems Ltd). Mice were fasted for overnight with free access to water *ad libitum* prior to PET scans. Mice were anaesthetized via inhalation of 5% isoflurane/oxygen gas mixture and placed on a pre-warmed mouse bed in the prone position. The tail of each mouse was warmed gently using warm water bath immediately before injection of ^{18}F–FDG (7.11±0.24MBq) via intravenous tail-vein injection. Mice were maintained using 2% isoflurane/oxygen during the 60mins uptake and imaging acquisition periods to reduce non-specific background uptake, and the body temperature were maintained in between 36.5 – 37.5°C during this time. A whole body, static PET acquisitions were performed for 20mins in 1:3 coincidence and normal count mode. Both T1- and T2-weighted MRI scans were performed for anatomical information and attenuation correction of PET images. The PET images were reconstructed using the vendor's reconstruction algorithm Tera-Tomo 3D (OSEM), with radionuclide decay, normalization, random, scatter, attenuation and dead time corrections applied to the data, resulting in a matrix of 0.3 mm^3. The PET and MR images were co-registered automatically, and data analyses were performed using InterView Fusion version 3.03.089.0000 (Mediso Medical Imaging Systems Ltd). For each

scan the volume of interest (VOI) of tumor or liver (with a radius of 3mm) were drawn manually in the PET images and presented as the standard uptake value (SUV). SUV was calculated using the equation: SUV = $C_{PET}(t)/(ID/BW)$, where $C_{PET}(t)$ is the measured activity in VOI, ID is the injected dose measured in kBq and BW is the mouse body weight in kg, assuming a tissue density of 1g/mL.

Statistical analyses. Statistical analyses were performed using GraphPad Prism 5.0 and SPSS 21.0. For comparison between two groups, statistical significance was determined by independent Student's *t*-test. For comparison between more than two groups, statistical significance was determined by one-way ANOVA with Tukey's post-hoc test. For *in vivo* animal studies, statistical significance was determined by repeated measures two-way ANOVA with Tukey's post-hoc test. Correlation of PRMT6 and PKM2 or p-ERK1/2 expression in clinical samples was evaluated by Fisher's exact test. Statistical significance defined as $p \leq 0.05$ with $*p<0.05$, $**p<0.01$ and $***p<0.001$. Number of animals included per group can be found in each respective figure. Data representative of 3 independent experiments unless otherwise specified.

RESULTS

PRMT6 deficiency in HCC results in enrichment of genes and metabolites involved in glycolysis. Recent work from our group has shown PRMT6 to be frequently down-regulated in human HCC and that PRMT6 functions to regulate cancer initiating and stemness activities (16). During generation of HCC cells with PRMT6 stably overexpressed or suppressed for the above experiments, we observed marked differences in the color of the culture medium. Specifically, cell culture media color showed increased acidity following knockdown of PRMT6 in HepG2 cells, while the reverse was observed when PRMT6 is overexpressed in MHCC97L cells (**Supplemental Figure S1A**). In culture media, phenol red exhibits a gradual color transition from red to yellow at lower pH values as a result of lactate production. This observation led us to hypothesize whether PRMT6 plays a role in modulating glucose metabolism. We began to explore the glycolytic capacity of PRMT6-modulated HCC cells. mRNA profiling of PRMT6 knockdown HCC cells identified a significant enrichment of genes closely associated with glycolysis, as compared to control cells (**Figure**

1A-B). Metabolome profiling using capillary electrophoresis time-of-flight mass spectrometry (CE-TOFMS) on the same cells revealed a number of key metabolites in glycolysis and the TCA cycle to be enhanced (**Figure 1C-E**). Specifically, knockdown of PRMT6 led to accumulation of intermediate metabolites in glycolysis including glucose-6-phosphate (G6P), fructose 1,6-bisphosphate (F1,6P), dihydroxyacetone phosphate (DHAP), 1,3-bisphosphoglyceric acid (1,3BPG), 3-phosphoglyceric acid (3PG), 2-phosphoglyceric acid (2PG), phosphoenolpyruvic acid (PEP), acetyl CoA and lactate. G6P: ribose 5-phosphate (R5P) ratio was also enhanced following knockdown of PRMT6. These changes suggested an enhancement of glycolysis without diversion of glucose into the pentose phosphate pathway (PPP). The amount of adenosine diphosphate (ADP) and adenosine triphosphate (ATP), which is the molecular unit of currency of intracellular energy transfer, also increased. Meanwhile, levels of TCA cycle metabolic intermediates derived from pyruvate/acetyl CoA and/or glutamine, including citrate, *cis*-aconitate, isocitrate, fumarate and malate also increased. This upsurge in ATP and TCA cycle intermediates suggest an increase in energy generation via TCA cycle through glucose/glutamine. Principal component analysis demonstrated that the extractions were consistent in the triplicates of each group (**Supplemental Figure S1B**). Increased glucose utilization after PRMT6 knockdown in HCC is evident in changes in both glycolysis and TCA cycle pathways, suggesting that PRMT6 contributes to glucose metabolic activities in HCC.

PRMT6 negatively regulates glycolysis in HCC. To test whether PRMT6 regulates glycolysis, we ablated PRMT6 expression in HepG2 with two distinct shRNAs, and stably overexpressed PRMT6 in MHCC97L cells as well as HCC patient-derived organoids (**Figure 2A; Supplemental Figure S2A**). Note that we have previously shown that knockdown of PRMT6 by shRNA showed similar tumor promotion effect as PRMT6 CRISPR-Cas9 knockout, with no off-target effects observed on other PRMT family members, suggesting a specific effect of PRMT6 on HCC cells (16). Knockdown of PRMT6 led to a significant increase of 2-NBDG uptake or glucose consumption, as well as lactate production and pyruvate kinase activity (**Figure 2B-D**). To better determine the involvement of PRMT6 in glycolysis-shifted metabolism in HCC, we also performed live monitoring using an extracellular flux analyzer for measurement of glucose-induced extracellular acidification rate (ECAR). Basal levels of ECAR at the beginning of measurements, which indicated non-glycolytic acidification, were low in HCC cells with or

without PRMT6 expression modulated. Equivalent ECAR was observed in the same cells both pre- and post-treatment with an ATP synthase inhibitor oligomycin to induce maximum cellular glycolytic capacity. At the final step, the addition of 2DG, an inhibitor for glycolysis, completely shut down extracellular acidification. Compared with control cells, knockdown of PRMT6 led to a significant increase in ECAR, a proxy for the rate of glycolysis and glycolytic capacity (**Figure 2E**). These changes are paralleled with a concomitant increase in expression of key glycolytic genes including GLUT1, LDHA and PKM2 (**Supplemental Figure S2B**). Conversely, stable PRMT6 overexpression in both MHCC97L and HCC patient derived organoids resulted in opposing effects (**Figure 2B-E; Supplemental Figure S2B**). Note that expression of other pyruvate kinase related genes including PKM1 and PKLR were not found to be altered upon modulation of PRMT6 expression (data not shown). To evaluate the regulation of glucose metabolism driven by PRMT6 *in vivo*, we injected MHCC97L cells with PRMT6 overexpressed into the liver of immunodeficient mice and measured radioactive glucose analogue ^{18}F-deoxyglucose (^{18}F-FDG) uptake by PET-MRI. Compared with control, mice injected with PRMT6 overexpressing cells developed smaller tumors (**Figure 2F; left**). More importantly, PRMT6 overexpression suppressed glucose uptake as indicated by reduced SUV_{max} of tumor and SUV ratio of tumor over liver background (**Figure 2F-G**). Collectively, this suggests PRMT6 negatively regulates glucose metabolism in HCC.

Catalytic activity of PRMT6 is required for regulating glycolysis in HCC. PRMT6 functions via catalyzing the asymmetric demethylation of arginine (ADMA) residues on proteins. Our previous work found knockdown and overexpression of PRMT6 to lead to a concomitant respective decrease and increase of ADMA, suggesting that the global arginine methyltransferase activity of these cells to be altered (16). To examine whether PRMT6 confers altered glycolytic properties in HCC through this enzymatic activity, we performed similar functional studies with wild-type PRMT6 or catalytic methyltransferase inactive mutant PRMT6$^{VLD:KLA}$ (17; **Supplemental Figure S2C**) overexpressed in MHCC97L cells (**Figure 2A; Supplemental Figure S2A**). We found the catalytic activity of PRMT6 to be important in conferring altered glycolytic abilities as ectopic overexpression of wild-type PRMT6 resulted in a significant decrease in glucose consumption, lactate production, pyruvate kinase activity, ECAR as well as expression of glycolytic related genes; while in contrast, a catalytic

methyltransferase inactive mutant of PRMT6 was unable to confer such functional phenotype (**Figure 2B-E; Supplemental Figure S2B**).

Methylation of CRAF at Arg100 by PRMT6 regulates expression and translocation of PKM2 into the nucleus via ERK-dependent signaling. Our earlier studies found PRMT6 to interact with CRAF on arginine 100 and as a result hinder its RAS binding potential and alter its downstream MEK/ERK signaling (16). There is now ample evidence to suggest that MEK/ERK signaling does alter both phosphorylation and nuclear translocation of PKM2 (18). In collaboration with other transcription factors, most notably hypoxia-inducible factor HIF-1α and c-myc, nuclear PKM2 induces glycolytic gene expression to promote glycolysis in cancer cells (19-20). This leads to our hypothesis that down-regulation of PRMT6 in HCC will enhance RAS/RAF binding via reduced methylation of CRAF at arginine 100 and subsequently heighten MEK/ERK signaling to promote PKM2 translocation into the nucleus to promote glycolysis (**Figure 3A**). As evidenced by Western Blot and immunofluorescence assays, knockdown of PRMT6 in HepG2 indeed led to heighted p-ERK1/2, p-PKM2 and PKM2 expression and localization in the nucleus, while overexpression of PRMT6 in MHCC97L and HCC patient derived organoid resulted in an opposing effect (**Figure 3B-C).** To quantify the degree of translocation of PKM2 after PRMT6 expression was modulated, we analyzed the immunofluorescence images by comparing the PKM2 signal intensity overlapping high DAPI staining region (i.e. nucleus) by ZEN 2 software. Higher intensity of PKM2 signal from the nucleus was observed following knockdown of PRMT6 in HepG2, while overexpression of PRMT6 in MHCC97L and HCC organoid resulted in opposing effects (**Supplemental Figure S3**). Consistently, overexpression of wild-type PRMT6, but not the catalytic inactive PRMT6 mutant, was able to suppress p-ERK1/2, p-PKM2, PKM2 expression and nuclear localization (**Figure 3B-C; Supplemental Figure S3)**. Nuclear localization of PKM2 following PRMT6 modulation was further substantiated by Western blot analysis of lysates collected from sub-fractionated cellular compartments (**Supplemental Figure S4A**). PKM2 exists in various oligomeric forms and dimeric PKM2 is the predominant form in the nucleus (18). Further analysis of cross-linked PKM2 revealed increased dimeric PKM2 following knockdown of PRMT6 in HepG2 and opposite observation in overexpression of PRMT6 in MHCC97L (**Supplemental Figure S4B**), which further substantiates relocalization of PKM2 into the nuclear following alteration of PRMT6.

To confirm that the effect of PRMT6-mediated relocalization of PKM2 was a result of methylation of CRAF at arginine 100, we compared the effect of overexpression of wild-type CRAF (CRAF WT) versus CRAF with arginine 100 residue mutated (CRAF R100K) on p-ERK1/2 expression as well as localization of PKM2. Overexpression of CRAF R100K resulted in heightened p-ERK1/2 expression (**Figure 3D**) and enhanced PKM2 expression in the nucleus (**Figure 3E, Supplemental Figure S4C-D**) of MHCC97L cells as compared to cells transfected with EV control or CRAF WT, as demonstrated by both immunofluorescence and Western Blot of cellular subfractionated protein lysates.

Inhibiting MEK/ERK signaling and PKM2 rescues the enhanced glycolysis observed in PRMT6 suppressed HCC cells. We also demonstrated the importance of MEK/ERK pathway in PRMT6-mediated relocalization of PKM2 by performing rescue experiments using a MEK-specific inhibitor U0126. U0126 suppressed PKM2 expression and nuclear localization conferred by PRMT6 knockdown (**Figure 4A-B, Supplemental Figure S5**). Note that dual color immunofluorescence for PKM2 and p-ERK1/2 expression also clearly identified the two to be localized together in the same cells (**Figure 4B**). In addition to monitoring localization of PKM2, we also carried out functional rescue experiments to validate the importance of the MEK/ERK pathway in PRMT6-mediated changes in glycolysis. U0126 suppressed the glycolytic properties conferred by PRMT6 knockdown, as evidenced by the diminished abilities of HCC cells to consume glucose (**Figure 4C**), produce lactate (**Figure 4D**), activate pyruvate kinase (**Figure 4E**), promote ECAR (**Figure 4F**) and enhance expression of glycolytic genes (**Figure 4G**).

Next, to investigate the exact role of PKM2 in PRMT6-mediated inhibition of HCC glycolysis, we co-expressed PKM2 shRNA (shPKM2) in PRMT6-depleted cells (**Figure 5A**) and determined the possibility of rescuing the metabolic effects observed in these cells. Functional glycolysis related assays confirmed that glucose consumption (**Figure 5B**), lactate production (**Figure 5C**), pyruvate kinase activity (**Figure 5D**) and ECAR (**Figure 5E**) levels, concomitant with GLUT1, LDHA and PKM2 expression (**Figure 5F**), were all substantially reduced in the double PRMT6/PKM2 knockdown cells compared with control cells, supporting the hypothesis that the glycolytic changes mediated by PRMT6 in HCC cells is

mostly likely due to the predominant expression of PKM2. Of note, depletion of PKM2 was sufficient to completely reverse increased aerobic glycolysis caused by PRMT6 depletion (**Figure 5E**). As an altered glucose metabolism has been associated with the growth and survival of cancer cells, we also examined the impact of PKM2 in PRMT6-depeleted HCC cells to respond to sorafenib, a FDA approved molecular targeted drug used in treatment of advanced HCC patients, and in tumor growth. Depletion of PKM2 in PRMT6-depleted HCC Huh1 cells sensitized cells to sorafenib (**Figure 5G**) and reduced tumorigenesis in an *in vivo* mouse model (**Figure 5H; Supplemental Figure S6**). Together, these results indicate that the enhanced glycolysis and resulting oncogenic properties observed in PRMT6-depleted cells is a consequence of MEK/ERK signaling and PKM2 activation.

PRMT6–MEK/ERK–PKM2 signaling axis deregulated in DEN+CCL_4 HCC-induced PRMT6 knockout mouse model as well as in human HCC clinical samples. To further substantiate our findings, we extended our analysis in a HCC mice model with endogenous PRMT6 expression depleted (17). Specifically, wild-type C57BL/6J and PRMT6 knockout ($PRMT6^{-/-}$) mice were subjected to DEN+CCL_4 treatment for induction of a fibrosis/inflammation-associated HCC model that closely mimics the disease in human. Our earlier work found $PRMT6^{-/-}$ mice to develop bigger HCC tumors than WT mice; while H&E staining also revealed larger areas of tumors in $PRMT6^{-/-}$ mice compared with controls (16). Relevant to this current study, we have now performed immunohistochemistry staining for PRMT6 and p-ERK1/2 on these xenografted liver sections; and analyzed PKM2 localization of these dissociated xenografted livers by Western Blot in dissociated tissues subfractionated for cytoplasmic and nuclear protein. Immunohistochemistry and Western Blot analyses showed absence of PRMT6, concomitant with stronger expression of pERK1/2 and higher nuclear PKM2 in the $PRMT6^{-/-}$ mice compared with WT mice, suggesting that our proposed PRMT6 – MEK/ERK – PKM2 pathway is indeed deregulated in this HCC immunocompetent mouse model with endogenous knockout of PRMT6 (**Figure 6A**).

In addition, we have also performed immunohistochemistry analysis to examine for expression of PRMT6, p-ERK1/2 and nuclear PKM2 in 31 pairs of non-tumor liver and HCC human clinical samples. Consistent with our previous findings (16), we found PRMT6 to be frequently down-regulated in HCC as compared to adjacent non-tumor liver. In addition, we

also found down-regulation of PRMT6 in HCC as compared to non-tumor liver to be significantly correlated with enhanced translocation of PKM2 into the nucleus; as well as enhanced p-ERK1/2 expression (**Figure 6B**).

PRMT6 deficiency in human HCC is regulated by hypoxia-responsive transcriptional repressor REST. One of the key characteristics in the tumor microenvironment is hypoxia, which has been shown to drive the Warburg effect. Interestingly, incubation of HCC cells, HepG2 and MHCC97L, in hypoxic condition (1% O_2) reduced the expression of PRMT6 (**Figure 7A, Supplemental Figure S7A**). HIF-1α is a key regulator of cellular response to hypoxia, which acts as a transcription activator to drive glycolysis. REST (repressor element 1-silencing transcription factor) has recently been shown to be a hypoxia-responsive transcriptional repressor under the control of HIF-1α (21). Notably, we observed a concomitant upregulation of REST along with attenuated PRMT6 expression under hypoxia (**Figure 7A; Supplemental Figure S7A)**. Furthermore, ENCODE also identified two potential binding sites of REST on the PRMT6 promoter (**Figure 7B**). We hypothesized that PRMT6 expression is negatively regulated by REST. We designed three truncated versions of the promoter region of PRMT6 which contained both 5' and 3' binding sites (FL), 3' binding site only (T1) and with both binding sites deleted (T2) (**Figure 7B**). Luciferase reporter assays found hypoxia to only suppress the transcription activity of cells transfected with FL and T1 constructs, suggesting the importance of the 3' binding site in hypoxia induced PRMT6 suppression (**Figure 7C**). ChIP enrichment assays showed increased REST binding to the 3' binding site in the PRMT6 promoter (**Figure 7D**). To understand the importance of REST in the regulation of PRMT6 expression, we performed rescue experiments with overexpression of dominant negative REST (REST DN), which only contains the DNA binding domain of REST. Induction of REST DN expression by doxycycline enhanced the expression of PRMT6 and transcription activity of PRMT6 promoter, as demonstrated by Western blot and luciferase reporter assays, respectively (**Figure 7E**). To further confirm the biological relevance of REST DN expression in HCC, we also completed a set of functional assays testing for altered sorafenib resistance and glycolysis. And indeed, induction of REST DN led to enhanced sensitivity to sorafenib as well as decreased glucose uptake, lactate production, pyruvate kinase activity as well as ECAR (**Supplemental Figure S7B-F**). We also elucidated the role of PRMT6 suppression in hypoxia induced glycolysis. We overexpressed PRMT6 in HCC cells

and performed functional glycolytic studies under normoxic and hypoxic conditions. Glucose uptake, lactate production and pyruvate kinase activity were increased in EV control cells cultured in hypoxic compared to normoxic condition. This increases in glucose metabolism could be reverted with PRMT6 overexpression (**Figure 7F, Supplemental Figure S7G**). Both glycolysis and glycolytic capacity of cells cultured in hypoxic condition was also significantly lower when PRMT6 was overexpressed (**Figure 7G**). This data suggests a novel regulatory mechanism of PRMT6 leading to enhanced glycolysis through PKM2 relocalization.

Glycolysis inhibitor 2DG sensitizes PRMT6 knockdown cells to sorafenib and reduces tumorigenesis. To examine the potential of targeting metabolic reprogramming in PRMT6 suppressed HCC cells, we performed rescue experiments with 2DG, a glycolysis inhibitor, and studied its effect on altering sorafenib response and tumorigenicity. Glucose uptake measurements confirmed concentration of 2DG used (10μM) for both HepG2 and Huh1 cells to significantly alter glucose uptake (**Supplemental Figure 8**). Functionally, addition of the same concentration of 2DG sensitized PRMT6 knockdown cells towards sorafenib (**Figure 8A**) and inhibited tumor growth (**Figure 8B-C**). This serves as a proof-of-concept that targeting glycolysis with a 2DG inhibitor can sufficiently reverse the resistance to sorafenib and increase in tumorigenesis of PRMT6 suppressed HCC tumors. Taken together, down-regulation of PRMT6 in HCC can drive Warburg effect to promote tumorigenicity and sorafenib resistance via methylation of CRAF at Arg100, thereby altering expression and translocation of PKM2 into the nucleus via an ERK-dependent manner. Notably, in a hypoxic tumor microenvironment, PRMT6 expression is further attenuated via the control of REST, which is a known hypoxia-responsive transcriptional repressor under the control of HIF-1α.

DISCUSSION

Aerobic glycolysis plays key roles in tumorigenesis and resistance to chemotherapeutics. However, the driver for switching to aerobic glycolysis in HCC is still unclear. We showed that reduced asymmetric arginine dimethylation on CRAF by PRMT6 promotes aerobic glycolysis using HCC cells and patients derived organoids *in vitro* and PET-MRI *in vivo*. This metabolic switch is driven by enhanced CRAF/MEK/ERK signaling leading to increased translocation of PKM2 into the nucleus, which in turn stimulates transcription of various glycolysis related genes including GLUT1, LDHA and PKM2. Silencing MEK/ERK signaling and PKM2 in PRMT6 suppressed cells completely reversed the enhanced aerobic glycolysis *in vitro* and tumorigenicity *in vivo*. The altered PRMT6–ERK–PKM2 signaling axis was further confirmed in both a HCC mouse model with endogenous knockout of PRMT6 as well as in HCC clinical samples. We also discovered an upstream regulator of PRMT6, REST, which acts as a transcription suppressor of PRMT6 in HCC cells. Finally, as a proof-of-concept, inhibition of glycolysis by 2DG reduced tumor growth *in vivo* and increased sensitivity of HCC cells towards first-line treatment sorafenib.

Our work suggests arginine methylation by PRMT6, a type I PRMT family member, to be a critical post-translational modification event regulating aerobic glycolysis in HCC. Post-translational modification of protein is influential in cancer and regulates protein activity, stability and localization through acetylation, methylation, phosphorylation and glycosylation, etc. However, research studying the link between metabolism and post-translational modification has mainly focused on histone modification in the past (22-23). In recent years, several type I PRMT family members have been linked with aerobic glycolysis in cancer and the importance of protein methylation on metabolism has been demonstrated in other model organisms, such as yeast and prokaryote (13-15, 24-25). During the preparation of this manuscript, Yan et al. also demonstrated PRMT6 methylates and thereby inhibits SIRT7, which epigenetically promotes mitochondria biogenesis and connects it to glucose availability in an AMPK-dependent manner (26). However, their study is focused more on sirtuin SIRT7 and how its methylation by PRMT6 connects glucose sensing with mitochondria biogenesis. Further, the study by Yan et al. was also not linked to the cancer disease. Here, our work pinpoints the importance of protein arginine methylation, via

PRMT6, in the regulation of aerobic glycolysis via PKM2 in HCC cells. The regulation of PKM2 has long been an interest as it is important for cancer survival including HCC (27-28). A recent paper shows activation of aerobic glycolysis through methylation of PKM2 by PRMT4, suggesting a link between post-translational modification and PKM2 activity (28). Here we show for the first time that post-translational modification of a protein upstream of PKM2 can also control the localization and therefore the expression of PKM2. This suggests a potential regulatory mechanism of PKM2 that has not been reported and can stimulate future development of drug for targeting PKM2 in HCC. We have shown that inhibition of MEK/ERK signaling with MEK inhibitor U0126 can reverse the translocation of PKM2 and therefore enhance glycolysis. Thus the use of an upstream inhibitor has the potential to regulate the metabolic reprogramming and tumorigenicity effect of PKM2.

Hypoxia is a hallmark event in cancer caused by poor vascularization in the core of tumor. It induces expression of a range of genes in which HIF-1α is the main effector. HIF-1α drives glycolysis via direct activation of transcription of several glycolysis related gene, including PKM2 (19, 29). Our work suggests a new pathway by which hypoxia induces glycolysis. We show that hypoxia stimulated expression of REST, a HIF-1α inducible gene, to serve as a transcriptional repressor for PRMT6. This suppression of PRMT6 then stimulates translocation of PKM2 into the nucleus and drives transcription of glycolysis related genes. Previous studies only focused on the direct effect of HIF-1α on PKM2 expression and the positive feedback loop on HIF-1α (19). We explored a new direction by which HIF-1α enhances PKM2 expression through REST/PRMT6 and therefore glycolysis. Indeed, we can reverse the hypoxia driven increased in glycolysis by overexpressing PRMT6, suggesting the importance of PRMT6.

2D cell culture model has been criticized for being not physiological due to the absence of 3D architecture. In our study, we used HCC patient-derived organoids, which have shown to develop 3D architecture similar to *in vivo* structure, to further confirm our observation from 2D cell culture model. Indeed, we observed a similar trend in studies overexpressing PRMT6 in 2D cell culture and 3D HCC patient derived organoids. In addition, the use of nutrient rich cell culture media does not represent the physiological nutrients level *in vivo*, which is fundamentally important in studying metabolism. To overcome this limitation, we also used

PET-MRI with ^{18}F-FDG to study the effect of PRMT6 expression on cancer cell metabolism *in vivo*. PET-MRI with ^{18}F-FDG has long been used in cancer patients to monitor cancer progression or treatment outcome. Using this state-of-the-art technique, our work shows that reduced glucose metabolism in tumor with PRMT6 overexpressed *in vivo*, substantiating our *in vitro* findings.

Current treatment for HCC yields unsatisfactory results. As a proof-of-concept, our work show the effectiveness of inhibiting glycolysis to increase sensitivity towards first-line treatment, sorafenib, in a subset of HCC patients with low PRMT6 expression. Since no specific PRMT6 activator is available for clinical use, our work reveals several novel points for intervention targeting PRMT6 suppressed HCC. We found REST, which is the upstream regulator of PRMT6, to be potentially targetable. REST suppresses transcription by recruiting a range of proteins including CoREST, HDACs, MeCP2 and Sin3. (30-31). Although we have yet to elucidate the detailed mechanism by which REST suppresses the expression of PRMT6, further studies of the mechanism by which REST suppresses PRMT6 may reveal insight for identifying potential targets for restoring PRMT6 expression in HCC. In addition, blocking of PKM2 translocation may also be effective in suppressing glycolysis. Notably, in a recent study, Liao et al. (2017) elegantly reported a robust system for *in vivo* activation of endogenous target genes through trans-epigenetic remodeling. The system relies on recruitment of Cas9 and transcriptional activation complexes to target loci by modified single-guide RNAs; and as a proof-of-concept, they used the technology to treat mouse models of diabetes, muscular dystrophy, and acute kidney disease (32). This approach can be considered for use in PRMT6 gene activation *in vivo* in HCC patients and as a combination treatment along with use of glycolysis inhibitors, for instance, to reverse Warburg effect in HCC.

REFERENCES

1. Cairns RA, Harris IS, Mak TW. Regulation of cancer cell metabolism. Nat Rev Cancer 2011; 11:85-95.
2. Hanahan D, Weinberg RA. Hallmarks of cancer: the next generation. Cell 2011; 144:646-674.
3. Kitamura K, et al. Proliferative activity in hepatocellular carcinoma is closely correlated with glucose metabolism but not angiogenesis. J Hepatol 2011; 55:846-857.
4. Tamada M, Suematsu M, Saya H. Pyruvate kinase M2: multiple faces for conferring benefits on cancer cells. Clin Cancer Res 2012; 18:5554-5561.
5. Wong CC, et al. Switching of pyruvate kinase isoform L to M2 promotes metabolic reprogramming in hepatocarcinogensis. PLoS One 2014; 9:e115036.
6. Christofk HR, et al. The M2 splice isoform of pyruvate kinase is important for cancer metabolism and tumor growth. Nature 2008; 452:230-233.
7. Bedford MT, Clarke SG. Protein arginine methylation in mammals: who, what and why. Mol Cell 2009; 33:1-13.
8. Blanc RS, Richard S. Arginine methylation: the coming of age. Mol Cell 2017; 65:8-24.
9. Larsen SC, et al. Proteome-wide analysis of arginine monomethylation reveals widespread occurrence in human cells. Sci Signal 2016; 9:rs9.
10. Onwuli DO, Rigau-Roca L, Cawthorne C, Beltran-Alvarez P. Mapping arginine methylation in the human body and cardiac disease. Proteomics Clin Appl 2017; 11:1-9.
11. Cheung N, Chan LC, Thompson A, Clearly ML, So CW. Protein arginine-methyltransferase-dependent oncogenesis. Nat Cell Biol 2007; 9:1208-1215.
12. Yang Y, Bedford MT. Protein arginine methyltransferases and cancer. Nat Rev Cancer 2013; 13:37-50.
13. Liu F, et al. PKM2 methylation by CARM1 activates aerobic glycolysis to promote tumorigenesis. Nat Cell Biol 2017; 19:1358-1370.
14. Yamamoto T, et al. Reduced methylation of PFKFB3 in cancer cells shunts glucose towards the pentose phosphate pathway. Nat Commun 2014; 5:3480.
15. Zhong XY, et al. CARM1 methylates GAPDH to regulate glucose metabolism and is suppressed in liver cancer. Cell Rep 2018; 24:3207-3223.

16. Chan LH, et al. PRMT6 regulates RAS/RAF binding and MEK/ERK-mediated cancer stemness activities in hepatocellular carcinoma through CRAF methylation. Cell Rep 2018; 25:690-701.
17. Neault M, Mallette FA, Vogel G, Michaud-Levesque J, Richard S. Ablation of PRMT6 reveals a role as a negative transcriptional regulator of the p53 tumor suppressor. Nucleic Acid Res 2012; 40:9513-9521.
18. Yang W, et al. Nuclear PKM2 regulates β-catenin transactivation upon EGFR activation. Nature 2011; 480:118-122.
19. Luo W, et al. Pyruvate kinase M2 is a PHD3-stimulated coactivator for hypoxia-inducible factor 1. Cell 2011; 145:732-744.
20. Yang W, et al. ERK1/2-dependent phosphorylation and nuclear translocation of PKM2 promotes the Warburg effect. Nat Cell Biol 2012; 14:1295-1304.
21. Cavadas MA, et al. REST is a hypoxia-responsive transcriptional repressor. Sci Rep 2016; 26:31355.
22. Yu J, Auwerx J. Protein deacetylation by SIRT1: An emerging key post-translational modification in metabolic regulation. Pharmacol Res 2010; 62:35-41.
23. Fan J, Krautkramer KA, Feldman JL, Denu JM. Metabolic regulation of histone post-translational modifications. ACS Chem Biol 2015; 10:95-108.
24. Brunk E, et al. Characterizing posttranslational modifications in prokaryotic metabolism using a multiscale workflow. Proc Natl Acad Sci USA 2018; 115:11096-11101.
25. Oliveira AP, Sauer U. The importance of post-translational modifications in regulating Saccharomyces cerevisiae metabolism. FEMS Yeast Res 2012; 12:104-117.
26. Yan WW, et al. Arginine methylation of SIRT7 couples glucose sensing with mitochondria biogenesis. EMBO Rep 2018; 19:e43677.
27. Iansante V, et al. PARP14 promotes the Warburg effect in hepatocellular carcinoma by inhibiting JNK1-dependent PKM2 phosphorylation and activation. Nat Commun 2015; 6:7882.
28. Liu Y, et al. Clinicopathological and prognostic significance of PKM2 protein expression in cirrhotic hepatocellular carcinoma and non-cirrhotic hepatocellular carcinoma. Sci Rep 2017; 7:15924.

29. Robey IF, Lien AD, Welsh SJ, Baggett BK, Gillies RJ. Hypoxia-inducible factor-1alpha and the glycolytic phenotype in tumors. Neoplasia 2005; 7:324-330.
30. Coulson JM. Transcriptional regulation: cancer, neurons and the REST. Curr Biol 2005; 15: R665-8.
31. Hwang JY, Zukin RS. REST, a master transcriptional regulator in neurodegenerative disease. Curr Opin Neurobiol 2018; 48:193-200.
32. Liao HK, et al. *In vivo* target gene activation via CRISPR/Cas9-mediated *trans*-epigenetic modulation. Cell 2017; 171:1495-1507.
33. Huch M, et al. Long-term culture of genome-stable bipotent stem cells from adult human liver. Cell 2015; 160:299-312.

AUTHOR CONTRIBUTIONS

TLW and SM conceived the project and designed the studies with assistance from LHC. TLW and KYN performed the research, analyzed and interpreted the data, with the help of LHC, LZ and NC. RH provided resources for Seahorse studies. TKL provided resources for Seahorse studies and critical scientific input. KVT and PLK performed the research, analyzed and interpreted the data relating to the PET-MRI *in vivo* studies. SR provided PRMT6 knockout mice as well as expertise on PRMT studies. CML and KM obtained patient consent and provided the clinical samples for organoid culture and expression correlation analysis. TLW and SM wrote the paper. SM supervised the project and provided funding for the study.

ACKNOWLEDGEMENTS

This project is supported in part by grants from the Research Grants Council of Hong Kong – General Research Fund (17143516 and 17105917), Theme Based Research Scheme (T12-710/16-R) and Collaborative Research Fund (C7018-14E). Stephanie Ma is a recipient of the Croucher Innovation Award from the Croucher Foundation. We thank the Faculty Core Facility (The University of Hong Kong) for providing and maintaining the equipment and technical support needed for flow cytometry, confocal microscopy and PET-MRI studies. We thank the Laboratory Animal Unit (The University of Hong Kong) for supporting our animal work studies. We thank the University Research Facility in Life Science, Hong Kong Polytechnic University for providing resources and equipment for Seahorse studies. We also thank the State Key Laboratory of Pharmaceutical Biotechnology for providing equipment for Seahorse studies.

FIGURE LEGENDS

Figure 1. PRMT6 deficiency in HCC results in enrichment of genes and metabolites involved in glycolysis. (A) Western blot analysis for PRMT6 expression in HCC HepG2 cells with or without PRMT6 repressed. **(B)** GSEA identified an enrichment of genes related to glycolysis in PRMT6 silenced HCC cells. Normalized enrichment score (NES), nominal (NOM) *p* value and false discovery rate (FDR) *q* value indicated. **(C)** Volcano plot of fold change (PRMT6 silenced over control) of all metabolites measured by CE-TOF MS. Dotted line represent absolute log2 fold change >0.5 (x-axis) and $p<0.05$ (y-axis). **(D-E)** Quantification of metabolic intermediates in glycolysis (D) and TCA cycle (E) by CE-TOF MS. Absolute values of metabolites shown. Data representative of three independent experiments. Bars and error represent mean ± SD of replicate experiments. Data compared between groups with independent Student's *t*-test. Abbreviations: NTC, scrambled non-target control; shPRMT6, shRNA targeted at PRMT6.

Figure 2. PRMT6 negatively regulates glycolysis in HCC. (A) Western blot analysis for PRMT6 expression in HCC cells and patient derived organoids with or without PRMT6 modulated, including knockdown and overexpression with wild-type (WT) or catalytic inactive mutant (Mut) constructs. **(B-D)** Measurements of glucose consumption (B), lactate production (C) and pyruvate kinase activity (D) in HCC cells and patient derived organoids with or without PRMT6 expression modulated, including knockdown and overexpression with WT or Mut constructs. *n* = 4 or more independent experiments. **(E)** ECAR (a proxy for the rate of glycolysis) in HCC cells and patient derived organoids with our without PRMT6 expression modulated, including knockdown and overexpression with WT or Mut constructs. *n* = 6 or more independent experiments. **(F)** Tumor volume, FDG uptake [standardized uptake value (SUV)] in tumor, and ratio of SUV of tumor and SUV of liver as measured by PET-MRI. **(G)** Representative axial PET−MRI images (tumors indicated by white arrows) and mouse whole-body maximum intensity projection (tumors indicated by black arrows) of nude mice bearing EV or PRMT6 overexpression tumors 60 minutes after intravenous injection of ^{18}F−FDG. *n* = 8-9 per group. For data presented in panels B-F, data compared to NTC or EV with independent Student's *t*-test for two groups or between groups with one-way ANOVA with Tukey's post-hoc test for three groups. Data shown as box plots with data point of each independent experiment. Abbreviations: NTC, scrambled non-target control; shPRMT6, shRNA targeted at PRMT6; KD1 and KD2, shPRMT6 knockdown clones 1 and 2; EV, empty vector control; WT, wild-type PRMT6; Mut, catalytic inactive mutant PRMT6.

Figure 3. Methylation of CRAF at Arg100 by PRMT6 regulates expression and translocation of PKM2 into the nucleus via ERK-dependent signaling. (A) Schematic illustration depicting proposed metabolic changes and its link to an altered CRAF/MEK/ERK signaling in the absence of PRMT6. **(B)** Western blot analysis for PRMT6, phosphorylated and total ERK, and phosphorylated (Ser37) and total PKM2 expression in HCC cells and patient derived organoids with or without PRMT6 modulated, including knockdown and overexpression with wild-type (WT) or catalytic inactive mutant (Mut) constructs. **(C)** Immunofluorescence staining of PKM2 in HCC cells and patient derived organoids with or without PRMT6 modulated. Scale bar = 20μm, except for the second row (4μm) which is a magnified version

of a selected field of images shown in the first row. DAPI to stain the nucleus. **(D)** Western blot analysis for CRAF, phosphorylated and total ERK expression in MHCC97L cells with empty vector (EV) control, wild-type CRAF (WT) or CRAF with arginine 100 mutation (R100K) overexpressed. **(E)** Immunofluorescence staining of PKM2 in MHCC97L cells with EV control, WT or R100K CRAF overexpressed. Scale bar = 20μm, except for the second column (4μm) which is a magnified version of a selected field of images shown in the first column. DAPI to stain the nucleus. Mean fluorescence intensity calculated by analyzing the average nucleus PKM2 intensity of 20 cells per experiment (*n* = 3 independent experiments). The intensity profile of PKM2 and DAPI recorded and presented as box plot. Data shown as box plots with data of each cell. Data compared between groups with one-way ANOVA with Tukey's post-hoc. Abbreviations: NTC, scrambled non-target control; shPRMT6, shRNA targeted at PRMT6; KD1 and KD2, shPRMT6 knockdown clones 1 and 2; EV, empty vector control; WT, wild-type PRMT6; Mut, catalytic inactive mutant PRMT6; CARF WT, wild-type CRAF; CRAF R100K, CRAF with arginine 100 mutated.

Figure 4. Inhibiting MEK/ERK signaling rescues the enhanced glycolysis observed in PRMT6 suppressed HCC cells. (A) Western blot analysis for PRMT6, phosphorylated and total ERK and phosphorylated (Ser37) and total PKM2 expression in HepG2 cells expressing NTC or shPRMT6, treated with control or MEK inhibitor U0126. **(B)** Dual color immunofluorescence analysis for phosphorylated ERK and PKM2 expression in HepG2 cells expressing NTC or shPRMT6, treated with control or MEK inhibitor U0126. Scale bar = 20μm, except for the second row (4μm) which is a magnified version of a selected field of images shown in the first row. DAPI to stain the nucleus. **(C-E)** Measurements of glucose consumption (C), lactate production (D) and pyruvate kinase activity (E) in HepG2 cells expressing NTC or shPRMT6, treated with control or MEK inhibitor U0126. *n* = 5 independent experiments. **(F)** ECAR in HepG2 cells expressing NTC or shPRMT6, treated with control or MEK inhibitor U0126. *n* = 8 independent experiments. **(G)** qPCR analysis for expression of glycolytic related genes including GLUT1, LDHA and PKM2 in HepG2 cells expressing NTC or shPRMT6, treated with control or MEK inhibitor U0126. *n* = 4 independent experiments. For data presented in panels C-G, data compared between groups with one-way ANOVA with Tukey's post-hoc test. Data shown as box plots with data point representative of each independent

experiment. Abbreviations: NTC, scrambled non-target control; shPRMT6, shRNA targeted at PRMT6; KD1 and KD2, shPRMT6 knockdown clones 1 and 2.

Figure 5. Silencing of PKM2 reverses the glycolytic changes mediated by PRMT6 in HCC cells. (A) Western blot analysis for PRMT6 and PKM2 expression in HepG2 cells co-expressing NTC or shPRMT6 clone KD2 and NTC or shPKM2 knockdown clones (588 and 494). **(B-D)** Measurements of glucose consumption (B), lactate production (C), pyruvate kinase activity (D) and ECAR (E) in HepG2 cells co-expressing NTC or shPRMT6 clone KD2 and NTC or shPKM2 knockdown clones. *n* = 4 independent experiments for panels B to D and *n* = 5 independent experiments for panel E. **(F)** qPCR analysis for expression of glycolytic related genes including GLUT1, LDHA and PKM2 in HepG2 cells co-expressing NTC or shPRMT6 clone KD2 and NTC or shPKM2 knockdown clones. *n* = 4 independent experiments. **(G)** Percentage of Annexin V-PI positive cells in HepG2 cells co-expressing NTC or shPRMT6 clone KD2 and NTC or shPKM2 knockdown clones in the presence of sorafenib. *n* = 4 independent experiments. **(H)** *Ex vivo* images of resected tumors and growth curves of tumor weight formed by subcutaneous injection of Huh1 HCC cells co-expressing NTC or shPRMT6 clone KD2 and NTC or shPKM2 knockdown clones. Scale bar = 1 cm. *n* = 6 mice per group. For data presented in panels B-G, data compared between groups with one-way ANOVA with Tukey's post-hoc test. Data shown as box plots with data point representative of each independent experiment. For data presented in panel H, data compared between groups with repeated measures two-way ANOVA with Tukey's post-hoc test. Bars and error represent mean ± SD of replicate experiments. Abbreviations: NTC, scrambled non-target control; shPRMT6, shRNA targeted at PRMT6; KD2, shPRMT6 knockdown clone 2; shPKM2, shRNA targeted at PKM2, 588 and 494, shPKM2 knockdown clones.

Figure 6. PRMT6–MEK/ERK–PKM2 signaling axis deregulated in DEN+CCL_4 HCC-induced PRMT6 knockout mouse model as well as in human HCC clinical samples. (A) Representative H&E and immunohistochemistry staining for PRMT6 and p-ERK1/2 expression of resected livers harvested from PRMT6 wild-type (WT) or knockout (KO) mice with DEN+CCL_4 induced HCC. Scale bar = 100μm. Quantitation of nuclear and cytoplasmic PKM2 levels by Western Blot using resected livers with cellular compartments sub-fractionated. *n* = 5 mice per group. Data compared to PRMT6 WT with independent

Student's *t*-test. Data shown as box plots with data point representative of each animal. **(B)** Representative immunohistochemistry staining for PRMT6, PKM2 and p-ERK1/2 expression of paired non-tumor liver and HCC human clinical samples (*n* = 31). Scale bar = 100μm. Tables below show number of cases for low or high PRMT6 expression relative to absent or present nuclear PKM2 expression and low or high p-ERK1/2 expression. Data compared between groups with Fisher's exact test. Abbreviations: WT, wild-type; KO, knockout; *ns*, not significant.

Figure 7. PRMT6 deficiency in human HCC is regulated by hypoxia-responsive transcriptional repressor REST. (A) Western Blot analysis for PRMT6 and REST expression in HepG2 and MHCC97L cells cultured in normoxic (21% O_2) and hypoxic (1% O_2) conditions for 24 or 48 hours. **(B)** Cloning strategy for luciferase reporter assay of PRMT6 promoter that consists two predicted REST binding sites. FL for full length. T1 and T2 for the two truncated mutants. **(C)** Luciferase reporter assays in HepG2 and MHCC97L cells cultured in normoxic and hypoxic conditions, transfected with PRMT6 FL and truncated mutants T1 and T2. pRL-TK *Renilla* luciferase plasmid co-transfected for normalization. *n* = 3 independent experiments. **(D)** Chromatin immunoprecipitation (ChIP) assays in HepG2 and MHCC97L cells cultured in normoxic and hypoxic conditions. *n* = 3 independent experiments. **(E)** Western Blot analysis for REST and PRMT6 expression and luciferase reporter assays in HepG2 and MHCC97L cells transfected with doxycycline inducible dominant negative REST (REST DN). *n* = 3 independent experiments. **(F)** Measurements of glucose consumption, lactate production and pyruvate kinase activity in MHCC97L cells expressing EV or PRMT6, cultured in normoxic or hypoxic conditions. *n* = 4 independent experiments. **(G)** ECAR in MHCC97L cells expressing EV or PRMT6, cultured in hypoxic condition. *n* = 5 independent experiments. For data presented in panels C-E and G, data compared to normoxic/-Dox/EV with independent Student's *t*-test. For data presented in panel F, data compared between groups with one-way ANOVA with Tukey's post-hoc test. Data shown as box plots with data point representative of each independent experiment. Abbreviations: EV, empty vector control; Dox, doxycycline; DN, dominant negative.

Figure 8. Glycolysis inhibitor 2DG sensitizes PRMT6 knockdown cells to sorafenib and reduces tumorigenesis. (A) Percentage of Annexin V-PI positive cells in HepG2 cells with or without PRMT6 expression silenced, in the presence or absence of 2DG and/or sorafenib. *n* = 4 independent experiments. Data compared between groups with one-way ANOVA with Tukey's post-hoc test. Data shown as box plots with data point representative of each independent experiment. **(B)** *Ex vivo* images of resected tumors and growth curves of tumor weight formed by subcutaneous injection of Huh1 HCC cells with or without PRMT6 expression silenced, in the presence or absence of 2DG. *n* = 6 per group. Scale bar = 1 cm. Data compared between groups with repeated measures two-way ANOVA with Tukey's post-hoc test. Bars and error represent mean ± SD of replicate experiments. **(C)** H&E and immunohistochemistry staining for PRMT6, PKM2 and p-ERK1/2 in tissue sections of resected Huh1 HCC xenografts. Scale bar = 100μm. Abbreviations: NTC, scrambled non-target control; shPRMT6, shRNA targeted at PRMT6; KD2, shPRMT6 knockdown clone 2; 2DG for 2-deoxy-D-glucose.

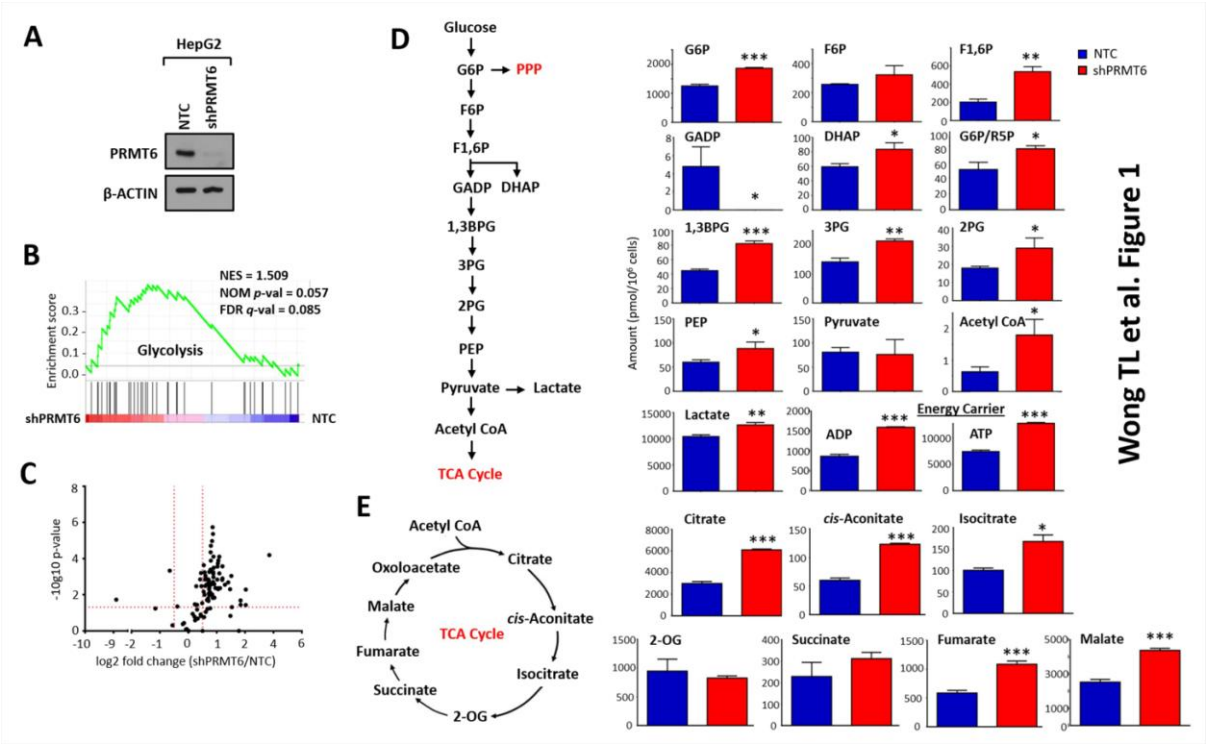

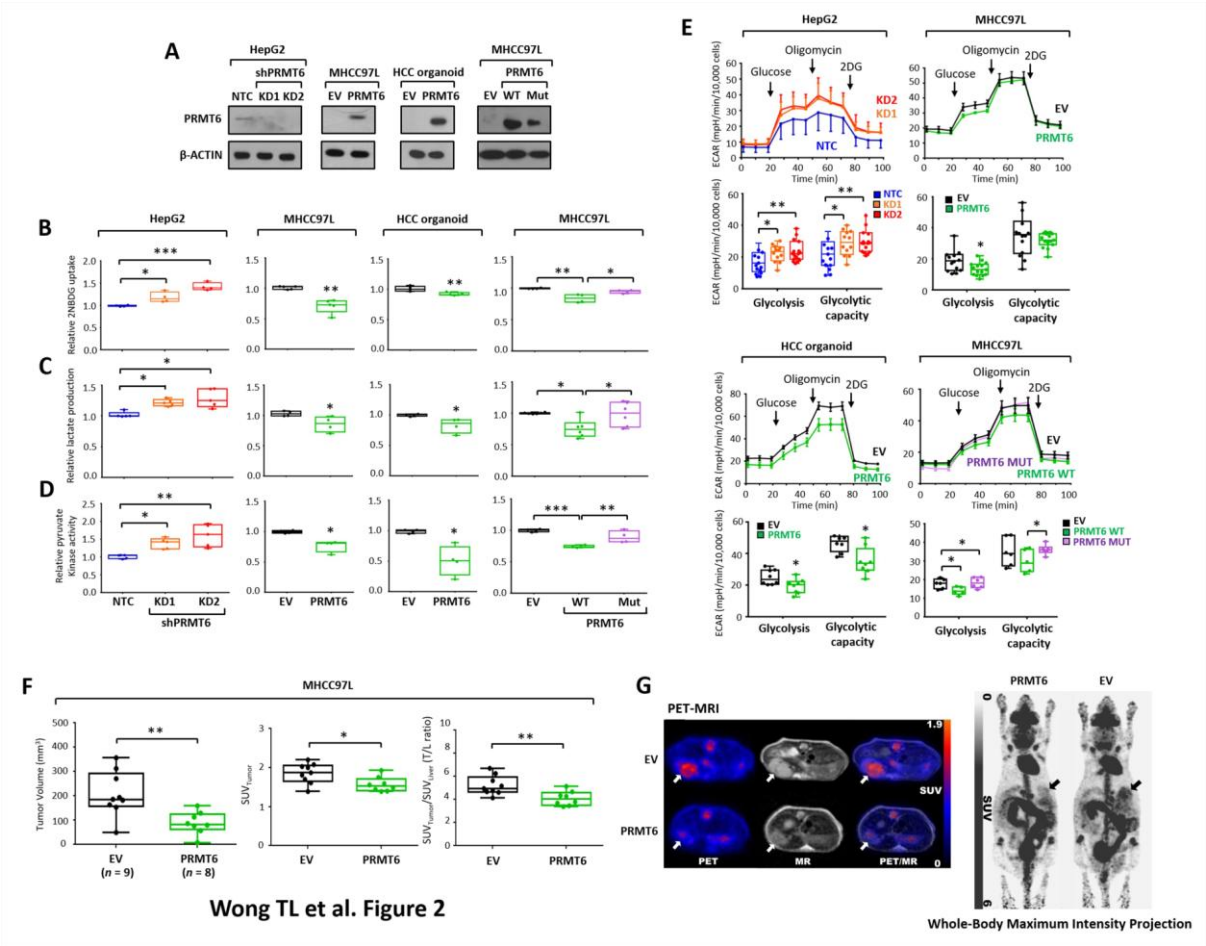

Wong TL et al. Figure 2

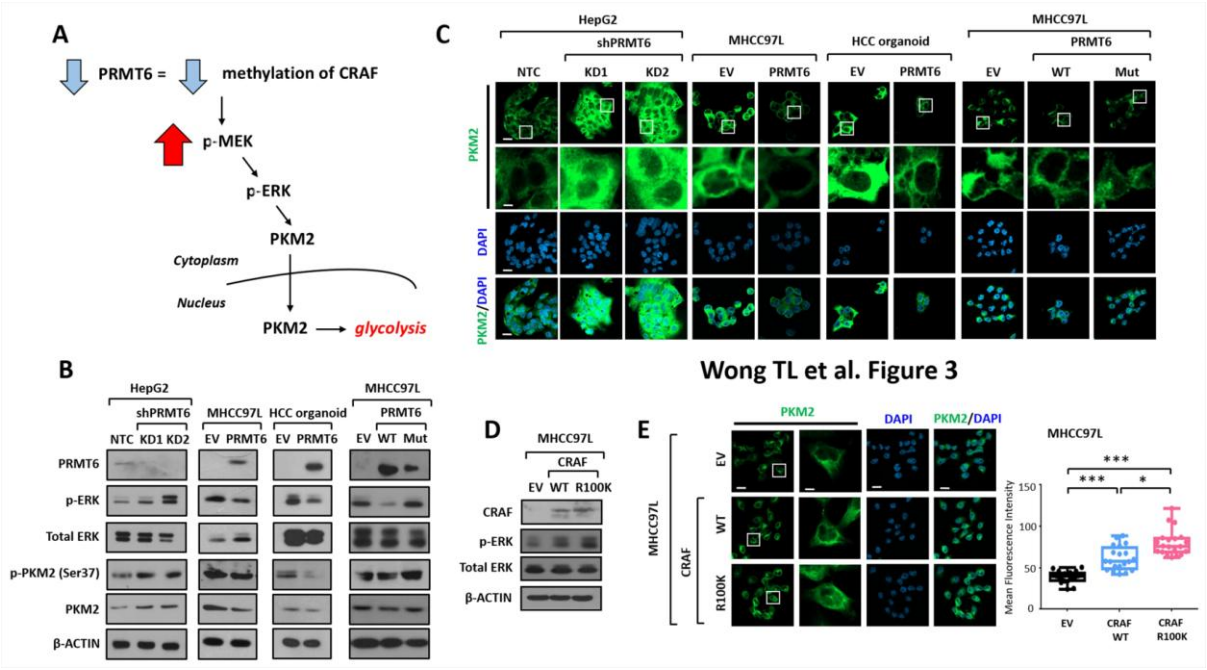

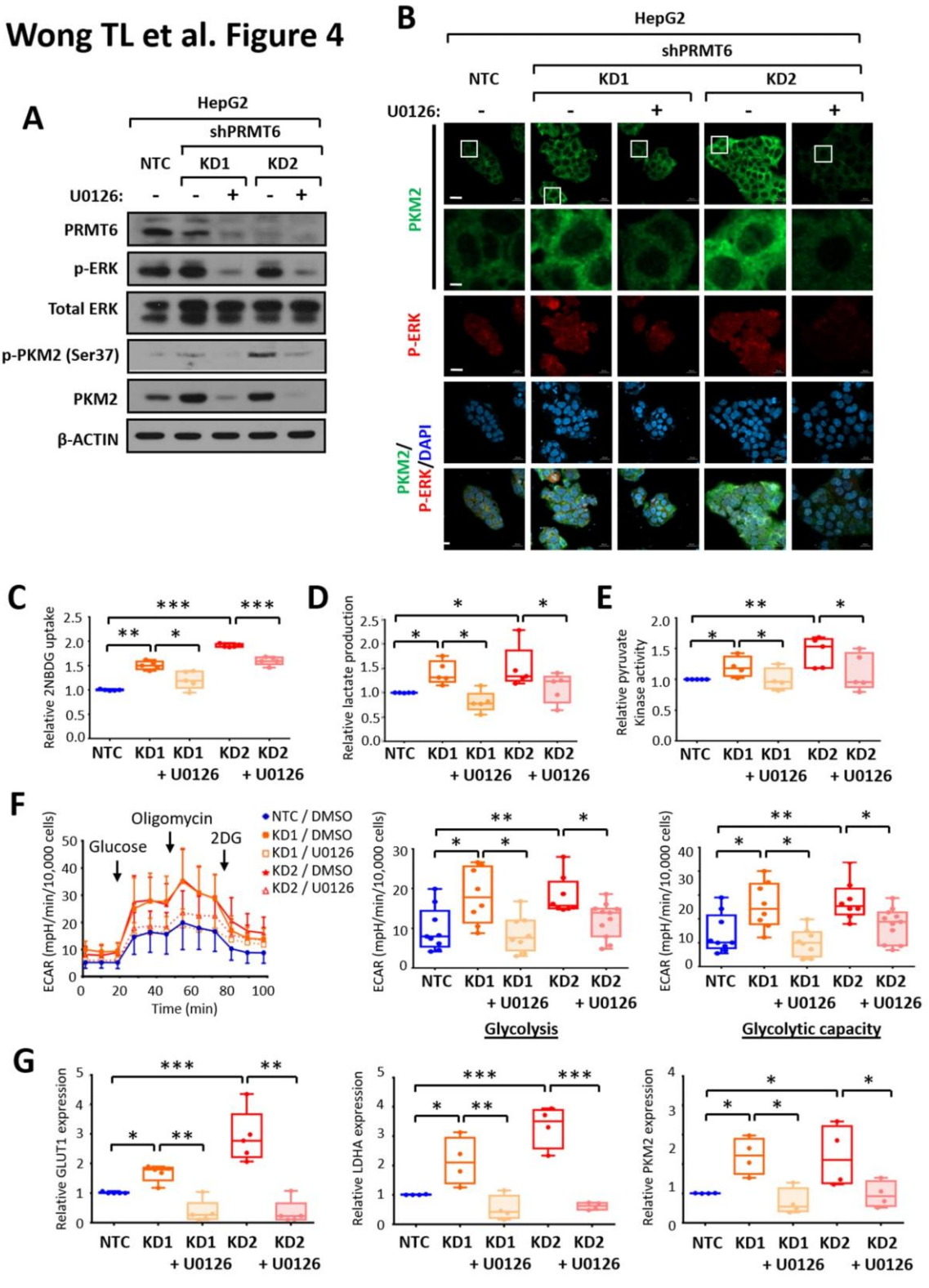

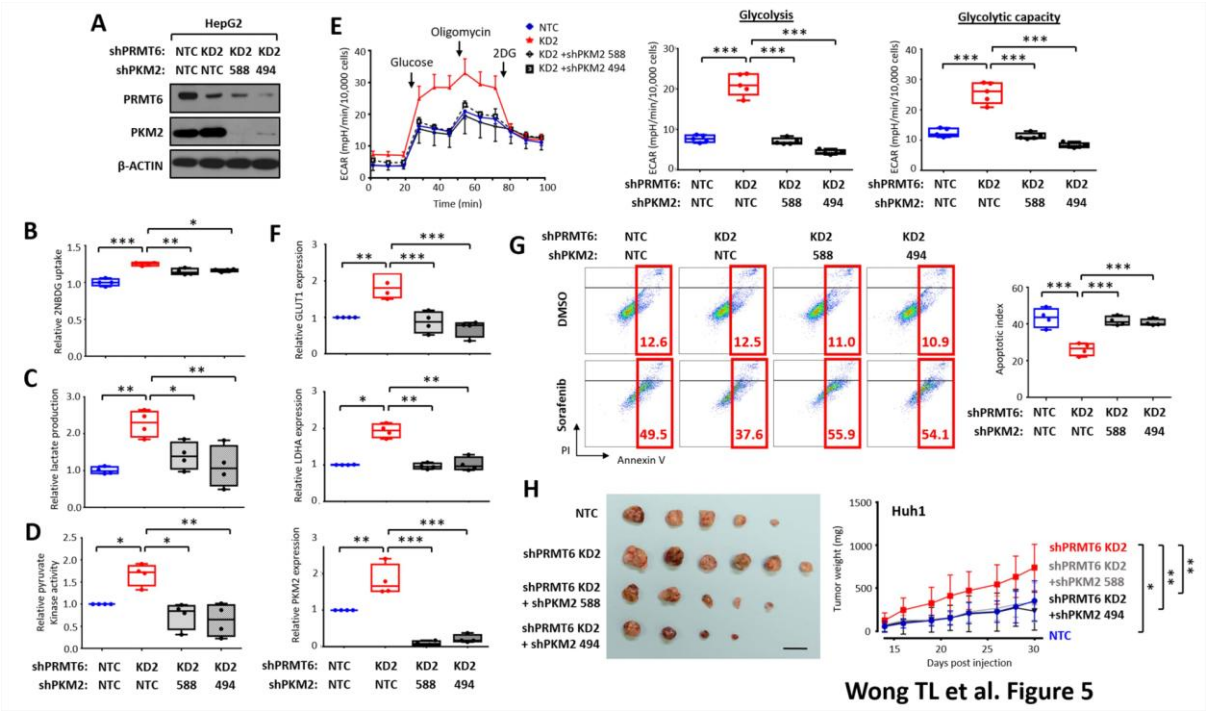

Wong TL et al. Figure 5

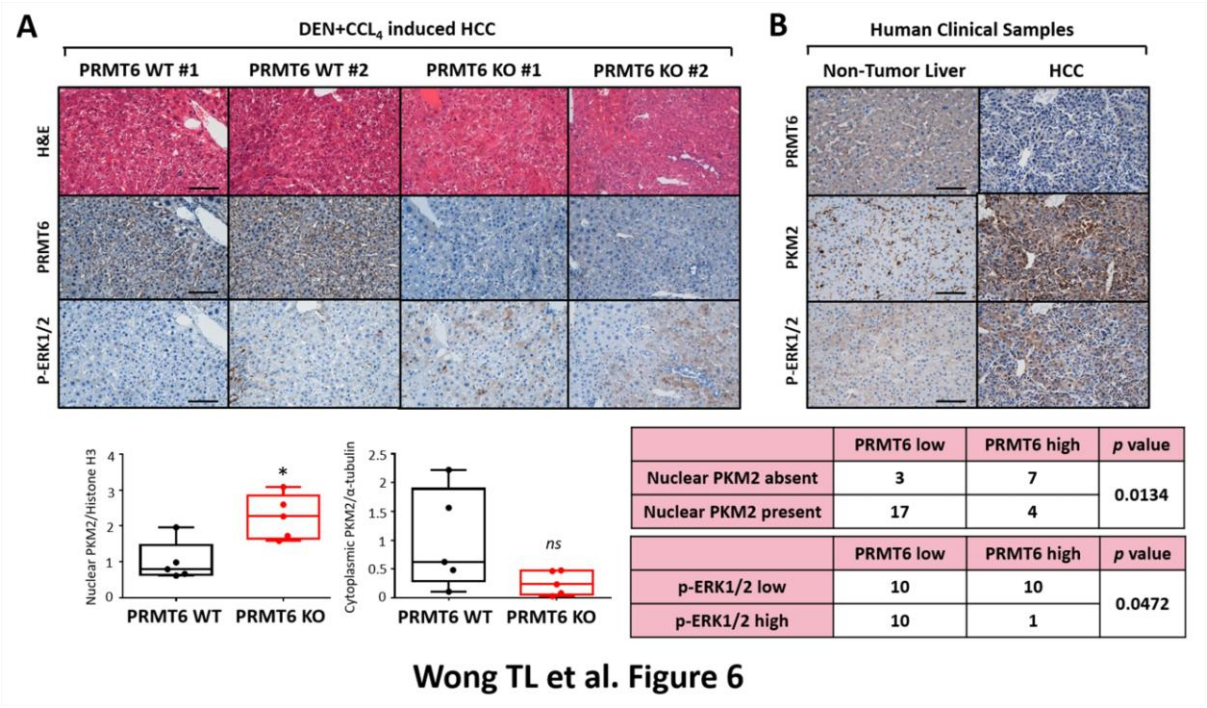

	PRMT6 low	PRMT6 high	*p* value
Nuclear PKM2 absent	3	7	0.0134
Nuclear PKM2 present	17	4	

	PRMT6 low	PRMT6 high	*p* value
p-ERK1/2 low	10	10	0.0472
p-ERK1/2 high	10	1	

Wong TL et al. Figure 6

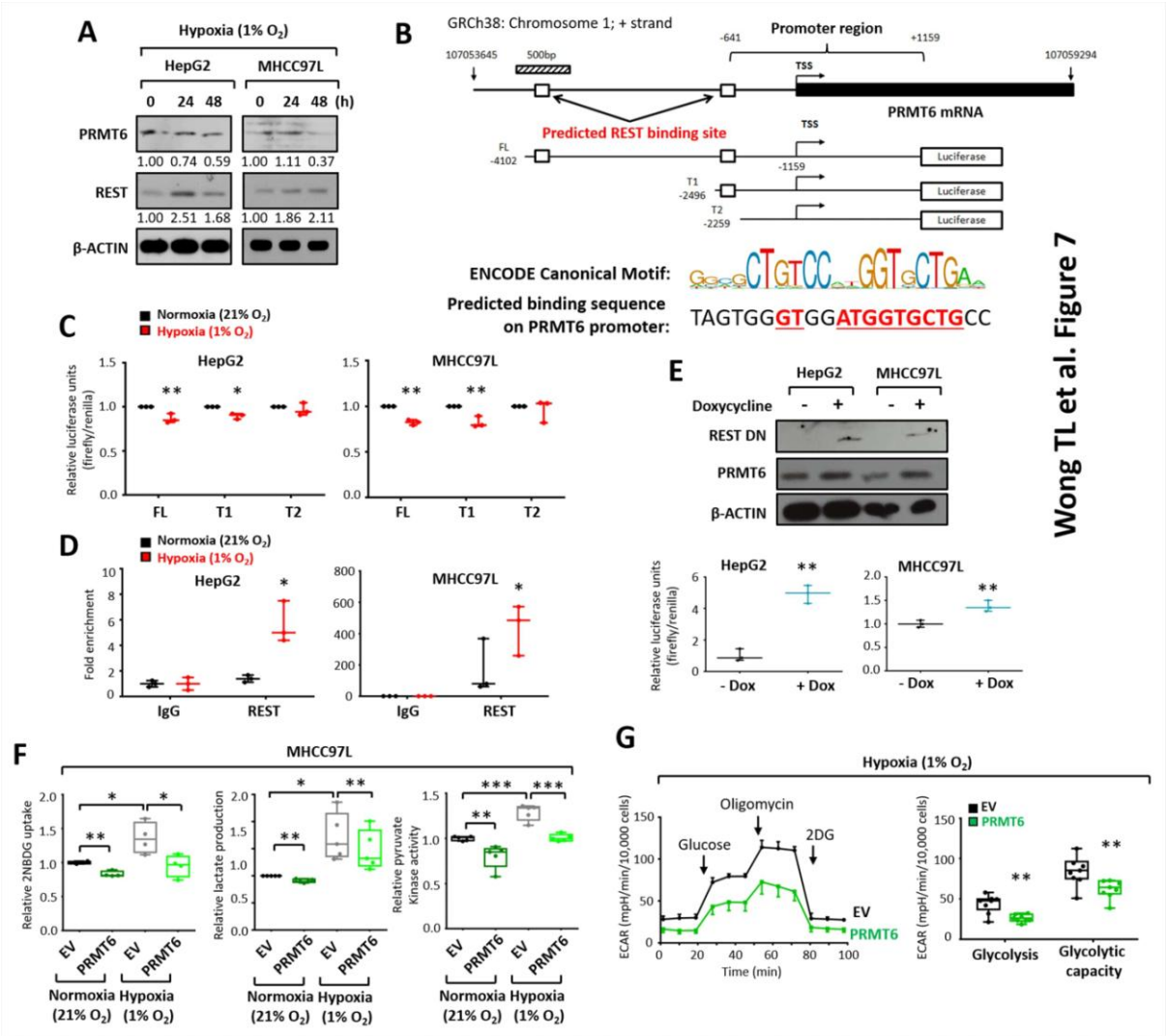

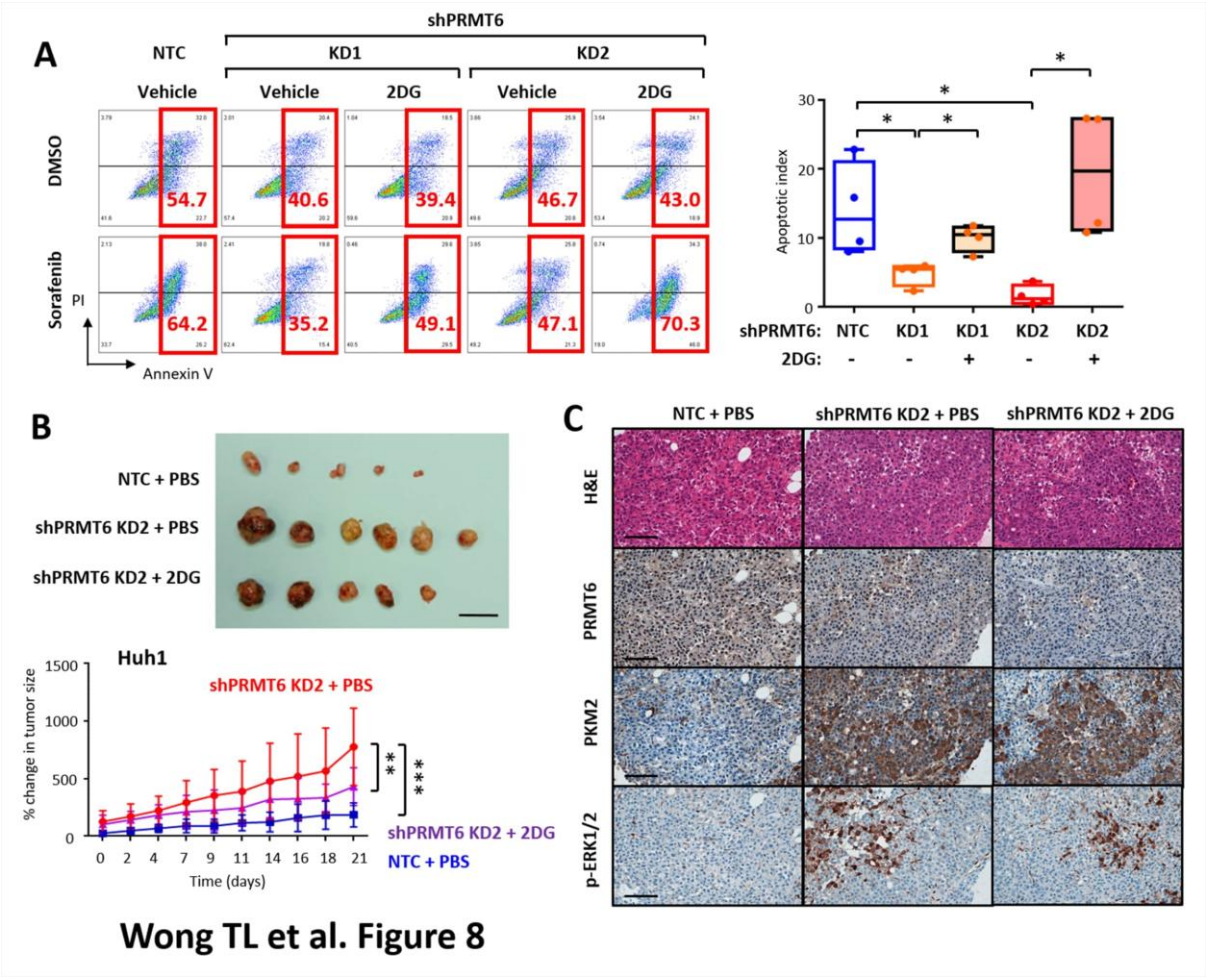

Wong TL et al. Figure 8